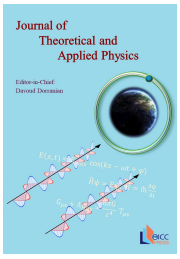

Volume 17, Issue 1, 172308 (1-7)

Journal of Theoretical and Applied Physics (JTAP)

https://dx.doi.org/10.57647/j.jtap.2023.1701.08

Impact of p-type semiconductor substrate on the transient response of metal-semiconductor-metal photodetector

Ali Barkhordari[1]*, Hamid Reza Mashayekhi[1], Şemsettin Altındal[2], Süleyman Özçelik[3,4], Yashar Azizian-Kalandaragh[2,5]*

[1]*Faculty of Physics, Shahid Bahonar University of Kerman, Kerman, Iran.*
[2]*Department of Physics, Faculty of Sciences, Gazi University, Ankara, Turkey.*
[3]*Department of Photonics, Faculty of Applied Sciences, Gazi University, Ankara, Turkey.*
[4]*Photonics Application and Research Center, Gazi University, Ankara, Turkey.*
[5]*Department of Physics, University of Mohaghegh Ardabili, Ardabil, Iran.*

*__Corresponding author__: alibarkhordari20@yahoo.com, yashar.a.k@gmail.com

Received 28 September 2022; Accepted 21 November 2022; Published online 28 November 2022

Abstract:
In this paper, using finite difference method, the effect of adding a *p*-layer at the back of a metal-semiconductor-metal (MSM) photodetector (PD) on the spatial electric charge distribution and the transient response of the device is numerically studied. To this aim, the fundamental equations of the semiconductor device, i.e., two current continuity time-dependent equations have been considered coupled with Poisson's equation. The I-V curve of the MSM photodetector is obtained as the main characteristics of each semiconductor device. Moreover, the variations of electrostatic potential, electron and hole concentrations are determined in the MSM photodetector with a *p*-layer at the back of the active layer. It is observed that the peak transient response of an MSM device is improved by back-gating the device as more electrons are injected to the semiconductor layer and the slower charge carriers (the holes) to be removed from the top circuit.

Keywords: MSM photodetector; p-type layer; Continuity and poisson's equations; Numerical solution; Finite difference method

1. Introduction

One of the most important parts of each optical communication system is a PD that is basically made of semiconductor materials [1, 2]. MSM configuration is well known to fabricate a PD which consists of a semiconductor as an absorbing layer and two metallic layers as the electrodes to make back-to-back Schottky diodes [3, 4]. This type of PD has a small intrinsic capacitance resulting in higher speed for large bit rate and higher sensitivity optoelectronic receivers than traditional *p-i-n* PDs [4]. Moreover, PDs with MSM structure exhibit a higher surface region in comparison with the *p-i-n* structures for the same thickness of active layer because of having a lateral design [5]. By studying the transient response of a MSM PD, two parts of the impulse response can be observed; a fast rise time and a long fall time. The fast rise time is the advantage of the device but the long fall time, due to the lower mobility of holes compared with electrons, leads to inter-symbol interference in the high-speed optical communications [6–8]. In order to reduce the fall time of the impulse response of the MSM PDs, the influence of the holes in the semiconductor layer should be diminished in the external circuit. For example, a technique that has been reported for this aim is intermediate temperature growth (ITG) of semiconductor material [9]. By using a gallium arsenide (GaAs) layer as an active layer, it was seen that the lifetime of charged carriers in the GaAs layer is only slightly more than the transient time between two metallic electrodes [10].
In addition, the effects of holes on the external circuit and the transient response of the PD are able to be decreased by either applying a negative voltage at the back of the

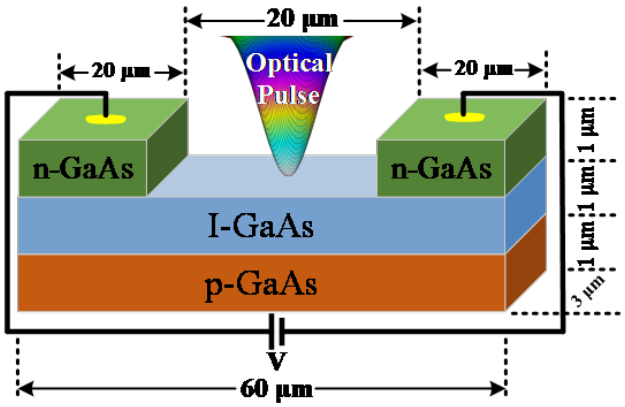

Figure 1. Schematic diagram of a MSM PD with a *p*-layer.

semiconductor layer or adding another semiconductor layer to effectively displace the charged carriers in the active layer [11]. Utilizing simulation techniques such as Newton iterative methods, finite element method (FEM), finite difference method (FDM), error estimation techniques, and adaptive mesh generation lead to finding the best way to fabricate a cost-effective device [2, 10–12].

In this work, the influence of a *p*-layer at the back of the semiconductor layer of MSM PD is investigated by implementing an algorithm based on the FDM to exactly solve the partial differential equations of the semiconductors using drift-diffusion approximation. After introducing the MSM structure with a *p*-layer at the back of the semiconductor in the next section, the governing equations, boundary conditions, discretization, and finally the solution methods are respectively expressed in the following. Since there are three unknown variables, i.e., n, p, and ψ, at each mesh point, therefore there are $3N$ unknowns for the N mesh points in two space dimensions. Newton's method has been considered to solve the systems of nonlinear continuity equations coupled to the Poisson equation for the $3N$ unknowns which arrange a one-column with $3N$ rows. In this arrangement, the first, second, and third N rows are assigned to n, p, and ψ variables, respectively. This procedure is discussed in more detail and has been applied to study the considered photodetector.

2. Model description

The MSM PD is a semiconductor device designed to detect optical pulses in the optical fiber communication systems. This PD is made from the GaAs semiconductor and consisted of two contacts on the top to detect high speed signals and one back layer designed for reducing the effect of the slow carriers, the low mobility hole carriers, on the high-speed top circuits by increasing the electron injection to the semiconductor as shown in Fig. 1.

Since the charge distribution and device characteristics for all parallel cross-sections in the active region and perpendicular to the contacts is the same, therefore the basic semiconductor equations are solved in a 2D plane containing the two top contacts and one *p*-layer. The two top contacts on the N region are Ohmic contacts that act as two rectifiers

Table 1. Doping concentration of different layers.

Layer	Doping concentration (m^{-3})
Top contacts (n-layers)	10^{24} n^+
I-GaAs	10^{20} n^-
p-layer	-10^{24} p^+

and show similar I-V characteristics as conventional MSM PD with Schottky contacts. The next layer is an intrinsic semiconductor of GaAs as long as the back layer of GaAs is the *p*-region in the structure. Table 1 represents the values of the doping concentration of different charged carriers in each layer.

The dimensions of a cross-section of the device containing two top N-region, I-region, and the *p*-layer are 60 μm width in x direction and 3 μm height of the three 1 μm thick N, I, and p layers in y-direction. The cross-section in the x-direction in the N region is 20 μm hence the gap between the two top contacts is 20 μm. Moreover, the profile of the cross-section in two dimensions is shown in Fig 2.

3. Governing equations

Based on the drift-diffusion approximation, the continuity equations coupled to the Poisson equation are able to describe the spatial and temporal behaviors of charged carriers (electrons and holes) in the semiconductor devices by applying an external electric field [9]. The Poisson equation in semiconductor could be written as:

$$\varepsilon_s \nabla^2 \psi = -q(n - p - N_d) \tag{1}$$

where, ε_s is the electrical permittivity of a semiconductor, ψ is the electrostatic potential, q is the elementary electron charge, n is electron number density, p is holes number density, and N_d is the impurities' concentration in a semiconductor.

Moreover, by considering the external generation mechanism, i.e., optical excitation, the time-dependent continuity equations are given as [11, 13]:

$$\frac{\partial n}{\partial t} - \frac{1}{q}\nabla . J_n = G_n - R_n \tag{2}$$

$$\frac{\partial p}{\partial t} - \frac{1}{q}\nabla . J_p = G_p - R_p \tag{3}$$

In the above equations, the flux densities of electron and hole (J_n and J_p) in drift-diffusion approximation can be defined as:

$$\mathbf{J}_l = \mu_l l \nabla \psi \pm D_l \nabla l, \;\; l = n, p \tag{4}$$

where $\pm$ are related to the electron and hole fluxes, respectively, D is the diffusion coefficient and μ is the mobility. Beer-Lambert's law represents the generation rate of photocarriers by dividing the total intensity of the absorbed light to the energy of a photon [14]. Therefore, the total intensity

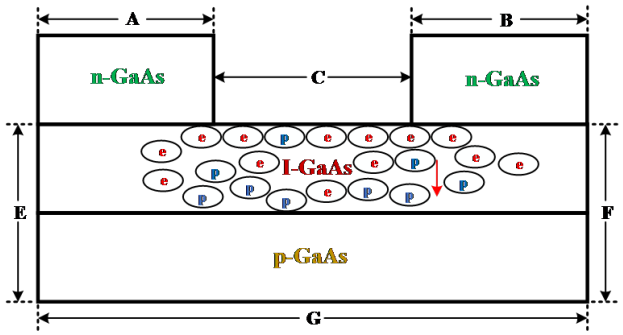

Figure 2. A cross-section of a MSM PD device with a p-layer.

of the absorbed light can be obtained by integrating on the z coordinate as:

$$G = G_n = G_p = \frac{\lambda\alpha}{hc}(1-R)(1-e^{-\alpha z})I_0(\mathbf{r},t) \qquad (5)$$

where λ, α, h, and c are the wavelength of the optical pulse, the absorption coefficient of the semiconductor layer, the Planck constant, and the light velocity in vacuum, respectively. R refers to the reflection coefficient of the surface of the semiconductor layer and $I_0(\mathbf{r},t)$ denotes the optical pulse intensity. A Gaussian profile centered at (x_0,y_0) with the total pulse duration equal to four times of the magnitude of the half of the FWHM (T_p), is considered in the space and time domains in this model as an optical pulse. Hence, the photocarrier density generated in the semiconductor surface layer due to irradiation of optical pulse can be calculated through the integration of the generation rate on the optical pulse duration as [14]:

$$n_{nn}(t_0) = \equiv P(t_0) = \int_0^{4T_p} G(x,y,t)dt = \frac{2\lambda\alpha p_{(z_0)}}{hcA_{eff}}(1-R)\times$$
$$(1-e^{-\alpha z|_{A_d}})e^{[-2\frac{(x-x_0)+(y-y_0)}{W_0^2}]}\int_0^{4T_p} -4\ln 2\left(\frac{t-2T_p}{T_p}\right)dt \qquad (6)$$

Here $p(z_0)$ is the power of the optical pulse, $A_{eff} = \pi W_0^2$ refers to the effective area of the laser beam with the waist of W_0, A_d denotes the depth of light absorption in the active layer of the photodetector. In addition, the non-radiative recombination rate, R, in the semiconductor devices due to Shockley-Read-Hall process could be expressed as [15]:

$$R = R_n = R_p = \frac{np - n_i^2}{\tau_n(n+n_i) + \tau_p(p+n_i)} \qquad (7)$$

where n_i refers to the intrinsic concentration in the semiconductor layer, τ_n and τ_p denotes the lifetime of electrons and holes, respectively [16].

Thus, the equations (1-3) must be numerically solved at each mesh point to simulate the considered MSM PD. However, initial guesses for n, p, and ψ at each mesh point together with applying proper boundary conditions to the device structure are needed. Moreover, the Dirichlet and Neumann boundary conditions appropriate to the structure of the presented MSM PD are considered which will be introduced in the following section.

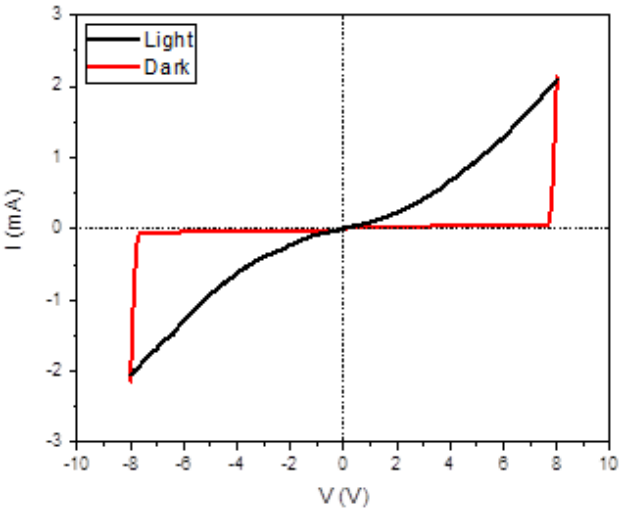

Figure 3. The I-V characteristic of MSM PD with a p-layer obtained from the two top contacts with and without light.

3.1 Boundary conditions

In general, the considered PD has a three-dimensional structure but using the device symmetry, its dimensions can be reduced into two dimensions. Fig. 2 shows a two-dimensional cross section of the presented MSM PD schematically.

The Dirichlet boundary condition is applied to the boundaries A, B and C where the contacts are considered as Ohmic contact. The charge neutrality condition at each contact and thermal equilibrium carrier concentration along with the Boltzmann distribution are assumed to define the boundary conditions. Table 2 presents the boundary conditions to be applied at each boundary in Figure 2. It must be noted that the constant C introduced in Table 2 (second column) is the potential gradient in the intermediate region and its value is obtained from the potential difference between the upper and the lower boundaries of the I-region divided by the corresponding distance between the two regions.

3.2 Scaling

To do the actual calculations in the PD simulation, the use of scaling factors is common in order to solve algorithms efficiently and, in some cases, to avoid numerical overflow or underflow [17]. Therefore, it is recommended to use scaled-down equations with similar quantities rather than particular constants with arbitrary values. The parameters ψ, n and p in the basic semiconductor equations attain values with different orders of magnitude in the regions with large and small space charges. The extremely large or small quantities make truncation errors in dealing with these parameters. Here, we use a simple scaling factor which is, from the mathematical point of view, more rigorous and introduced in [18–20]. Therefore, by multiplying equations (1) in ε/qn_{d_0}, (2) in $x_0^2/D_0n_{d_0}$, and (3) in $x_0/-qD_0n_{d_0}$, the considered equations will be non-dimension.

Table 2. Details of boundary conditions used in the simulation procedure [8-12].

Boundary	Dirichlet condition	Neumann condition
A	$\psi=\psi_a+\frac{kT}{q}\ln[\frac{n_d}{2n_i}+\sqrt{\frac{n_d^2}{4n_i^2}+1}],\ \mathbf{J}_n.\hat{n}=0,\ \mathbf{J}_p.\hat{n}=0$	$\partial\psi/\partial\mathbf{n}=0,\ \partial n/\partial\mathbf{n}=0,\ \partial p/\partial\mathbf{n}=0$
B	$\psi=\psi_a+\frac{kT}{q}\ln[\frac{n_d}{2n_i}+\sqrt{\frac{n_d^2}{4n_i^2}+1}],\ \mathbf{J}_n.\hat{n}=0,\ \mathbf{J}_p.\hat{n}=0$	$\partial\psi/\partial\mathbf{n}=0,\ \partial n/\partial\mathbf{n}=0,\ \partial p/\partial\mathbf{n}=0$
C	$\psi=0,\ n=0,\ p=0$	$\partial\psi/\partial\mathbf{n}=c,\ \partial n/\partial\mathbf{n}=0,\ \partial p/\partial\mathbf{n}=0$
E	$\psi=0,\ n=0,\ p=0$	$\partial\psi/\partial\mathbf{n}=c,\ \partial n/\partial\mathbf{n}=0,\ \partial p/\partial\mathbf{n}=0$
F	$\psi=0,\ n=0,\ p=0$	$\partial\psi/\partial\mathbf{n}=c,\ \partial n/\partial\mathbf{n}=0,\ \partial p/\partial\mathbf{n}=0$
G	$\psi=\psi_a+\frac{kT}{q}\ln[-\frac{n_d}{2n_i}+\sqrt{\frac{n_d^2}{4n_i^2}+1}],\ \mathbf{J}_n.\hat{n}=0,\ \mathbf{J}_p.\hat{n}=0$	$\partial\psi/\partial\mathbf{n}=0,\ \partial n/\partial\mathbf{n}=0,\ \partial p/\partial\mathbf{n}=0$

3.3 Discretization

In this section, the basic semiconductor equations in partial differential forms will be discretized and transformed to algebraic forms. By providing mesh points and assigning a pair of indices (i, j), we then can write the governing algebraic equations for each mesh point. So, using the five-point finite difference approximation, Poisson equation could be written as:

$$\left(\frac{\varepsilon\psi}{x_0^2qnd_0}\right)\left\{\begin{array}{l}\frac{\frac{\psi_{i+1,j}-\psi_{i,j}}{h_i}-\frac{\psi_{i,j}-\psi_{i-1,j}}{h_{i-1}}}{\frac{h_i+h_{i-1}}{2}}+\\ \\ \frac{\frac{\psi_{i,j+1}-\psi_{i,j}}{k_i}-\frac{\psi_{i,j}-\psi_{i,j-1}}{k_{j-1}}}{\frac{k_j+k_{j-1}}{2}}\end{array}\right\}-n_n|_{i,j}+n_p|_{i,j}+n_d|_{i,j}=0 \tag{8}$$

where h_i and k_j represent the distance from one mesh point to the neighboring ones in x and y directions, respectively. In order to perform the discretization of the continuity equations, they must be written in terms of current density components at mid interval points. Therefore, the electron and hole continuity equations can be respectively discretized as:

$$\frac{(t)|_{i+\frac{1}{2},j}-(t)|_{i-\frac{1}{2},j}}{\frac{m_i+m_{i-1}}{2}}+\frac{(-J_{nx})|_{i+\frac{1}{2},j}-(-J_{nx})|_{i-\frac{1}{2},j}}{\frac{h_i+h_{i-1}}{2}}+$$
$$\frac{(-J_{ny})|_{i,j+\frac{1}{2}}-(-J_{ny})|_{i,j-\frac{1}{2}}}{\frac{k_j+k_{j-1}}{2}}-G(\psi,n,p)|_{i,j}-R(\psi,n,p)|_{i,j}=0 \tag{9}$$

$$\frac{(t)|_{i+\frac{1}{2},j}-(t)|_{i-\frac{1}{2},j}}{\frac{m_i+m_{i-1}}{2}}+\frac{(J_{px})|_{i+\frac{1}{2},j}-(J_{px})|_{i-\frac{1}{2},j}}{\frac{h_i+h_{i-1}}{2}}+$$
$$\frac{(J_{py})|_{i,j+\frac{1}{2}}-(J_{py})|_{i,j-\frac{1}{2}}}{\frac{k_j+k_{j-1}}{2}}-G(\psi,n,p)|_{i,j}-R(\psi,n,p)|_{i,j}=0 \tag{10}$$

In addition, by considering the Einstein mobility-diffusion relation and Bernoulli function [13], the mid interval values for the current density components can be obtained. Besides, the x and y components of electrons and holes current density can be determined as:

$$J_{lx}|_{i\pm\frac{1}{2},j}=\pm D_l|_{i\pm\frac{1}{2},j}\frac{B\left(\frac{\psi_{i,j}-\psi_{i\pm1,j}}{vt}\right)l_{i,j}-B\left(\frac{\psi_{i\pm1,j}-\psi_{i,j}}{vt}\right)l_{i\pm1,j}}{h_{(i\pm\frac{1}{2})-\frac{1}{2}}} \tag{11}$$

$$J_{ly}|_{i,j\pm\frac{1}{2}}=\pm D_n|_{i,j\pm\frac{1}{2}}\frac{B\left(\frac{\psi_{i,j}-\psi_{i,j\pm1}}{vt}\right)l_{i,j}-B\left(\frac{\psi_{i,j\pm1}-\psi_{i,j}}{vt}\right)n_{i,j\pm1}}{k_{(j\pm\frac{1}{2})-\frac{1}{2}}} \tag{12}$$

where l represents n and p due to electron and hole number density. Moreover, it has been assumed that the current density has an intermediate value of $J_{lx}|_{(i\pm1/2,j)}$ in the interval $x\in[x_i,x_{i\pm1}]$ and $J_{ly}|_{(i,j\pm1/2)}$ in the interval $y\in[y_i,y_{i\pm1}]$. Also, the electrostatic potential is constant in the considered path. Furthermore, $G(\psi,n,p)|_{i,j}$ and $R(\psi,n,p)|_{i,j}$ could be defined as:

$$G(\psi,n,p)|_{i,j}=n_n(t_0)|_{i,j}\equiv n_p(t_0)|_{i,j} \tag{13}$$

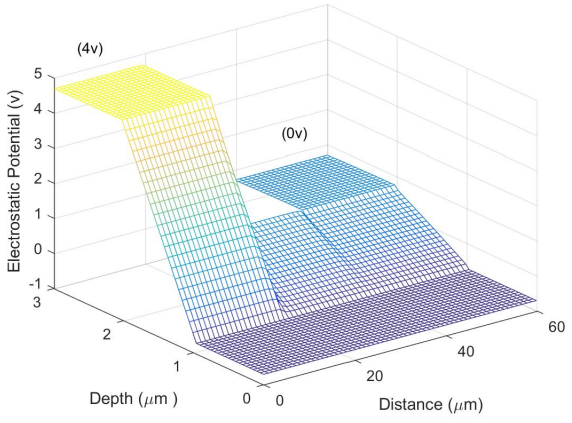

Figure 4. Electrostatic potential profile of the MSM PD when a p-layer is backed the active layer in steady-state condition.

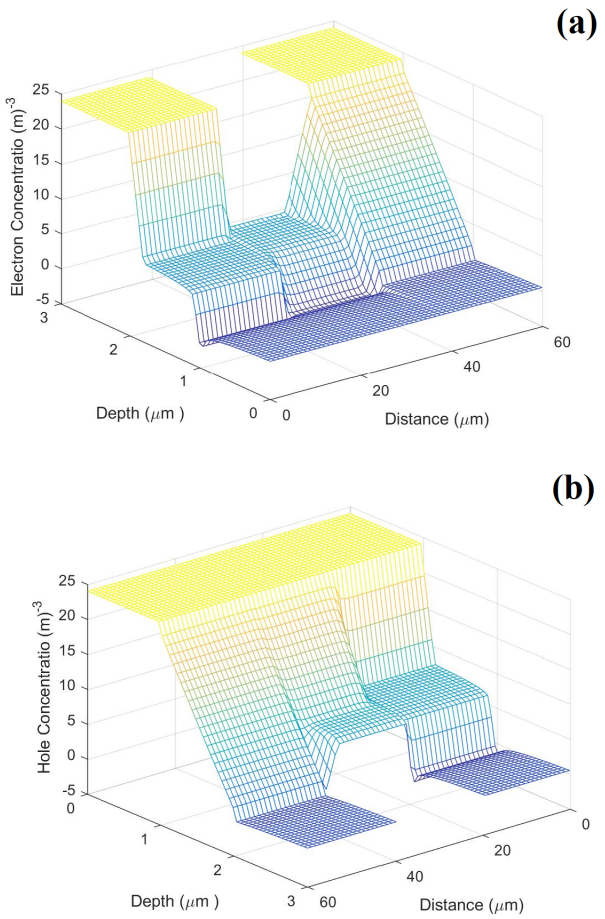

Figure 5. The logarithmic profiles of (a) electrons and (b) holes concentration in the MSM PD with a *p*-layer at the back of active layer.

$$R(\psi,n,p)|_{i,j} = \frac{n_n|_{i,j} n_p|_{i,j} - n_i^2}{\tau_n(n_n|_{i,j} + n_i) + \tau_p(n_p|_{i,j} + n_i)} \qquad (14)$$

As a result, by substituting the relations (11-14) into equations (9) and (10), the discretized form of the continuity equations is obtained.

3.4 Solution method

So far, many iteration methods have been proposed to solve the linear or nonlinear systems of algebraic equations derived from the basic semiconductor time-dependent equations [10-12]. In all these methods, the equations were solved either at each mesh point one by one in isolation or as a system of linear algebraic equations for the whole mesh points all together. In some methods also, only one of the equations is solved for one of the unknown variables by assuming that the other two variables are known at the given mesh point [15]. In the method that we introduce here as a novel technique, all three equations are solved simultaneously for all three unknowns of all mesh points. In other words, assigning N points on the device, the total of $3N$ coupled nonlinear algebraic equations are solved for the $3N$ unknown variables. The Newton iterative method is used for solving these equations. The $3N$ coupled nonlinear algebraic equations are formed by putting the linear Poisson's equation as the first N set and two current continuity equations for electrons and holes as the other two N sets of systems of nonlinear algebraic equations.

In order to make systems of nonlinear algebraic equations, we assign a number from 1 to N to each mesh point neglecting those on Dirichlet boundaries where the values of ψ, n, and p are known. Since we have N mesh points and at each mesh point there are three unknown variables ψ, n, and p, therefore $3N$ nonlinear algebraic equations must be written for the introduced PD.

The approach used here is to arrange the $3N$ unknowns in a one-column matrix as shown in (15). As can be seen from this matrix, the first N rows, the second N rows, and finally the third N rows are allocated for ψ, n, and p unknowns variables, respectively.

$$X = \begin{pmatrix} x_1 \\ x_2 \\ . \\ . \\ . \\ x_N \\ x_{N+1} \\ x_{N+2} \\ . \\ . \\ . \\ x_{2N} \\ x_{2N+1} \\ x_{2N+2} \\ . \\ . \\ . \\ x_{3N} \end{pmatrix} = \begin{pmatrix} \psi_1 \\ \psi_2 \\ . \\ . \\ . \\ \psi_N \\ n_1 \\ n_2 \\ . \\ . \\ . \\ n_N \\ p_1 \\ p_2 \\ . \\ . \\ . \\ p_N \end{pmatrix} \qquad (15)$$

The subscript indices of 1 to N correspond to the N points of the mesh on the device geometry. To form a system of nonlinear algebraic equations as shown in (16), we take into account the first N equations as the N linear algebraic Poisson's equation, the second N equation as the N nonlinear algebraic electron continuity equation, and the third N equations as the N nonlinear algebraic hole continuity equations.

$$F = f_i(x_1, x_2, ..., x_{3N}) = 0 \qquad (16)$$

Finally, we solve the system of nonlinear algebraic equations in (16) for i from 1 to $3N$ using Newton's iteration method. So, by assigning suitable initial guesses for ψ, n, and p arranged in a one-column with $3N$ rows, the corrections Δx corresponding to $\Delta\psi$, Δn, and Δp are calculated via Jacobean system using Taylor expansion of F:

$$\left(\frac{\partial F}{\partial X}\right)(\Delta X) = \begin{pmatrix} \frac{\partial f_\psi}{\partial \psi}|_{1,2,...,N} & \frac{\partial f_\psi}{\partial n_n}|_{1,2,...,N} & \frac{\partial f_\psi}{\partial n_p}|_{1,2,...,N} \\ \frac{\partial f_n}{\partial \psi}|_{1,2,...,N} & \frac{\partial f_n}{\partial n_n}|_{1,2,...,N} & \frac{\partial f_n}{\partial n_p}|_{1,2,...,N} \\ \frac{\partial f_p}{\partial \psi}|_{1,2,...,N} & \frac{\partial f_p}{\partial n_n}|_{1,2,...,N} & \frac{\partial f_p}{\partial n_p}|_{1,2,...,N} \end{pmatrix} \times$$

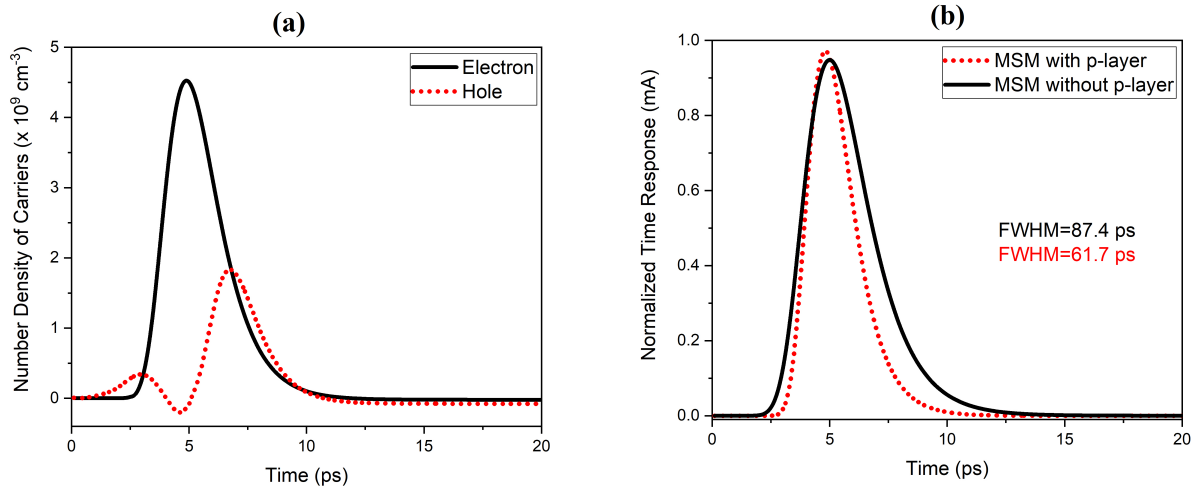

Figure 6. The transient profiles of (a) charged carriers and (b) current density in MSM PD with a p-layer at the back of the active layer.

$$\begin{pmatrix} \Delta\psi|_{1,2,\ldots,N} \\ \Delta n_n|_{1,2,\ldots,N} \\ \Delta n_p|_{1,2,\ldots,N} \end{pmatrix} = \begin{pmatrix} f_{0\psi}|_{1,2,\ldots,N} \\ f_{0n}|_{1,2,\ldots,N} \\ f_{0p}|_{1,2,\ldots,N} \end{pmatrix} \tag{17}$$

The Jacobi matrix of the system consists of nine parts, a single-diagonal and five off-diagonal elements. The solutions are updated by $X^{k+1} = X^k + \Delta X^k$ and $t^{k+1} = t^k + \Delta t^k$ in space and time domains, respectively. Moreover, the solution of the nonlinear algebraic equations system is sought after k iterations by checking the $X^{k+1} - X^k \leq 10^{-4}$ m and $t^{k+1} - t^k \leq 10^{-6}$ s criteria.

Table 3. Scaling factors.

Quantity	Symbol	Value
$\mathbf{x}$	x_0	$\max(x-y),\ \ x,y \in D$
ψ	ψ_0	kT/q
n,p,d	d_0	$\max\lvert d(x)\rvert,\ \ x \in D$
D_n, D_p	D_0	$\max\Big(D_n(\mathbf{x}), D_p(\mathbf{x})\Big),\ \ \mathbf{x} \in D$
μ_n, μ_p	-	D_0/ψ_0
G, R	-	$D_0 d_0/x^2$
T	-	x_0^2/D_0

4. Numerical results

In this section, the results of solving basic semiconductor time-dependent equations are presented based on the introduced FD algorithm for the MSM PD with a p-layer. It must be noted that a 30×50 uniform mesh including the gap area and boundaries are established for the simulation. Excluding the nodes or points for Dirichlet boundary condition, the total of N = 1730 points are considered for solving the equations. The left and right top contacts are biased by 4V and 0V, respectively. Using Newton's iteration method to solve the 3×1730 nonlinear algebraic equations, the solution was obtained after 10 iterations with convergence criteria in the simulation domain.

The I-V characteristics curve between the two top contacts of MSM PD with p-layer with and without light is shown in Fig 3. As can be seen, the results are the same as that of two back-to-back connected Schottky diodes and are what is expected from any MSM PD. In this calculation, the applied voltages are less than 12 V and that the ionization-impact phenomenon has not been considered. This result shows that our method could reproduce the experimental I-V characteristics of a MSM PD as given in [8] to a reasonably high degree of accuracy.

The electrostatic potential profile of the MSM PD biased by a voltage of 4 V with a p-layer on the back of the active layer is shown in Fig. 4. It should be mentioned that the electrostatic potential is calculated using the Dirichlet boundary condition for the two top contacts and p boundary region. As can be seen, the electrostatic potential of left-top-contact has increased by an amount of 4 V with respect to the built-in-potential whereas the other two contacts, i.e., right-top-contact and p remained at theirs built-in-potential value of ±0.7033 V, respectively. The validity of this calculation can be checked by noticing the electrostatic potential of the left-top-contact-Intrinsic-P region or right-top-contact-Intrinsic-P region are the same as the electrostatic potential of a p-i-n diode in equilibrium condition, respectively.

Additionally, logarithmic profiles of the electrons and holes density of the MSM PD are shown in Fig. 5 (a) and (b), respectively. The electron and hole densities in left- and right-top contacts and P regions have their equilibrium values because the Fermi levels in these regions do not change. It can also be seen from Fig. 5(a) that the electrons concentration in the I-region is reduced because of the positive voltage applied to left-top contact. However, as can be seen from Fig. 5(b), the holes concentration in the I-region is increased because holes are injected into this region as a result of positive voltage applied to left-top contact. The electrons and holes concentration in the P-Intrinsic-right-top-contact region remain in their equilibrium values since no voltage has been applied to right-top contact and P region.

In addition, the temporal response of the MSM PD with a *p*-layer at the back of the semiconductor is illustrated in Fig. 6(a). As shown, the variations of the electron density have a sharp peak but the density of holes slightly reduces before reaching its maximum value. Finally, Fig. 6(b) shows the time evolution of the total current density through the semiconductor layer of MSM PD. It is clear that the total current density is initially increased till 5 ps and then reduced from its peak value when the optical pulse is imposed at the middle of the semiconductor layer of the MSM PD. When a *p*-layer is placed at the back of the active layer of MSM PD, the electrons diffuse into the whole of the semiconductor layer and therefore, more electrons are injected into the external circuit. Indeed, the slower photocarriers (the holes) move toward the *p*-layer because it is negatively biased with respect to the zero bias top contact. The speed of the photodetector is significantly increased by this process due to the creation of more electron-hole pairs in the semiconductor layer of the device and removing more slow charge carriers from the two-top-contact circuitry.

5. Conclusion

In this paper, a FD numerical method was used to study the effect of *p*-layer at the back of the active layer on the spatial and temporal distributions of charge carriers in the MSM PD by solving the Poisson's equation and the time-dependent continuity equations. In this method, the equations were solved simultaneously as a nonlinear system of equations for ψ, n, and p variables corresponding to the electric potential, electrons and holes number density, respectively. The results obtained for the electrostatic potential, electrons, and holes concentration have a reasonably high degree of accuracy in comparison with those presented in the literature. Moreover, the transient response of the device was calculated by this method. It is found that the presence of *p*-layer at the back of the active layer of MSM PD causes more injection of the electron from the external circuit to the semiconductor layer, resulting in the diffusion of the electrons in the whole semiconductor layer, and hence, the creation of electron-hole pairs was increased. In addition, when one of the top contacts has higher potential with respect to the other one, the electric potential of the back-gated *p*-layer is negative with respect to the lower electric potential top contact and resulting in the removal of holes from the top contacts' circuit. Therefore, the speed of MSM PD is significantly enhanced by more producing the electron-hole pairs in the active layer of PD and taking out the slower charge carriers from the top circuit.

Conflict of interest statement
The authors declare that they have no conflict of interest.

References

[1] C. H. Chen, Y. H. Tsai, S. Y. Tsai, and C. F. Cheng. *Japanese Journal of Applied Physics*, **50**:04DG19, 2011.

[2] S. G. Rudi and S. Soleimani-Amiri. *Materials Science in Semiconductor Processing*, **150**:106918, 2022.

[3] J. S. Young, W. L. Ji, J. S. Changa, P. Y. Chen, and M. S. Peng. *Semiconductor Science and Technology*, **23**:085016, 2008.

[4] S. Y. Chu, T. H. Yeh, C. T. Lee, and H. Y. Lee. *Materials Science in Semiconductor Processing*, **142**:106471, 2022.

[5] A. Müller, G. Konstantinidis, M. Dragoman, D. Neculoiua nd A. Kostopoulos, M. Androulidakia, M. Kayambaki, and D. Vasilache. *Applied Optics*, **47**:1, 2008.

[6] F. Xie, H. Lu, D. J. Chen, X. Q. Xiu, H. Zhao, R. Zhang, and Y. D. Zheng. *IEEE Electron Device Letters*, **32**:1260, 2011.

[7] Ş. Altındal, A. Barkhordari, Y. Azizian-Kalandaragh, B. S. Çevrimli, , and H. R. Mashayekhi. *Materials Science in Semiconductor Processing*, **147**:106754, 2022.

[8] M. Patel, P. M. Pataniya, and C. K. Sumesh. *Materials Science in Semiconductor Processing*, **148**:106778, 2022.

[9] S. W. Seo and N. M. Jokerst. *Electronics Letters*, **43**:15, 2007.

[10] V. Krishnamurthy, M. C. Hargis, and M. R. Melloch. *IEEE Photonics Technology Letters*, **12**:1, 2000.

[11] A. Barkhordari, H. R. Mashayekhi, and Y. Azizian-Kalandaragh. *Physica B: Condensed Matter*, **596**:412406, 2020.

[12] A. Habibpoor and H. R. Mashayekhi. *Journal of Physics: Conference Series*, **286**:PH8, 2011.

[13] S. M. Sze, Y. Li, and K. K. Ng. *Physics of Semiconductor Devices*. John wiley and sons, 4th edition, 2021.

[14] C. Korman and I. D. Mayergoyz. *Journal of Applied Physics*, **68**:1324, 1990.

[15] A. Bea-Lev. *Semiconductors and Electronic Devices*. Prentice-Hall International, 2th edition, 1984.

[16] F. Masszi, P. A. Tove, and J. H. Bohline. *IEEE Transactions on Electron Devices*, **ED-33**:1379, 1986.

[17] D. Vasileska and S. M. Goodnick. *Computational Electronics*. Morgan and Claypool publishers, 1th edition, 2006.

[18] A. B. Vasil'eva and V. G. Stel'makh. *Math*, **17**:2, 1997.

[19] V. F. Butuzov and A. B. Vasila'eva. *Singularly Perturbed Equation in Critical Case, , 1978*. 1th edition, 1978.

[20] P. A. Markowich and C. A. Ringhofer. *SIAM Journal on Applied Mathematics*, **44**:101137, 1984.